2

Flows in Porous Media

2.1 Use Simple Methods First

We now turn our attention to the results that constitute the core of modern research on convective heat and mass transfer through porous media. Our objective is not only to organize the compact presentation of these results, but also to explain their origin. We want to show the student how to anticipate these results and the results for related problems. This is why we begin with methodology. We emphasize the freedom that educators and researchers have in choosing methods to solve problems, present the results, and put results into practice.

The field of convection in porous media is an excellent candidate for stressing this important message. It is mature enough, and at the same time it is rich: its results cover a wide spectrum of problems and applications in thermal engineering, physics, geophysics, bioengineering, civil engineering, and many other fields. These fields are united by several key phenomena, some of which are selected for review in this chapter. The opportunity that the maturity of our field offers is this: after a few decades of development, we find that more than one method is available for attacking a certain problem. Older methods, such as analysis and experiments (direct laboratory measurements), are as eligible to be used as the newer methods based on computational analysis. The point is that the available methods *compete* for the researcher's attention. The researcher has the freedom to choose the method that suits him or her (Bejan, 1995a).

Methods are literally competitive because each is an example of a tradeoff between cost (effort) and accuracy. The simpler methods require less effort and produce less accurate results than the more complicated methods. The researcher enters the marketplace of methodology with a personal profile: talent, time to work, interest in details, and users of the results of the contemplated work (e.g., customers, students). The match of researcher, problem, and method is not the result of chance. It is an optimization decision (structure, configuration) in the sense of *constructal* theory and design (Bejan, 2000). This

configuration maximizes the performance (benefit) for all parties concerned. The intellectual work that goes on in research and education is a conglomerate of mind–problem–method matches of the kind illustrated in this book. The so-called "knowledge industry" thrives on the optimization of matches and connections—it thrives on the development (growth) and optimization of structure.

Among the methods that have emerged in fluid mechanics and heat transfer, scale analysis (scaling) is one of the simplest and most cost effective (Bejan, 1984, 1995a); see Sections 2.1, 2.5, and 4.4. Scaling is now used by many, yet the need to explain its rules and promise remains. To accomplish this in a compact and effective format is the first objective of this chapter. Scale analysis is so cost effective that it is beneficial as a first step (preliminary, prerequisite) even in situations where the appropriate method is more laborious and the sought results are more accurate. The results of scale analysis serve as a guide. They tell the researcher what to expect before the use of a more laborious method, what the ultimate (accurate) results mean, and how to report them in dimensionless form. The engineering advice to "try the simplest first" fits perfectly in the optimization of research.

The second objective of this chapter is to explain the rules and the promise of another simple method: the intersection of asymptotes (Section 2.11). This method was born by accident, in the search for a quick solution to a homework problem, namely, the optimal spacing between parallel plates with natural convection (Bejan, 1984, problem 11, p. 157). What led to the quick solution is an idea of more permanent and general value: when one is challenged to describe a complicated system or phenomenon (e.g., a flow structure), it is helpful to describe the phenomenon in the simpler extremes (asymptotes) in which it may manifest itself. The complicated phenomenon lies somewhere between the extremes, and its behavior may be viewed as the result of the competition (clash, collision) between the extremes. This idea has helped us in many areas. For example, the highly complicated relations between the thermodynamic properties of a real substance (e.g., steam tables) make more sense when viewed as the intersection of two extremes of thermodynamic behavior: the incompressible substance model and the ideal gas model.

Although newer than scaling, the intersection of asymptotes method is now used frequently in thermal design and optimization (e.g., Sadeghipour and Razi, 2001). Optimization of global performance is an integral part of the physics of flow structures: flows choose certain patterns (shapes, structures, regimes) as compromises between the available extremes. Flows design for themselves paths for easiest access (Bejan, 2000). To illustrate this constructal characteristic of natural flows, in Section 2.11 we take a look at the classical phenomenon of natural convection in a porous layer saturated with fluid and heated from below (Horton and Rogers, 1945; Lapwood, 1948). This phenomenon has been investigated with increasingly accurate analytical, numerical, and experimental tools, as shown by recent reviews [e.g., Nield and Bejan (1999)]. Just like scaling, the intersection of asymptotes method

provides a surprisingly direct alternative, a short cut to the most important characteristics of the flow.

2.2 Scale Analysis of Forced Convection Boundary Layers

Scaling is a method for determining answers to concrete problems, such as the heat transfer rate in a configuration that is described completely. The results are correct and accurate, but only in an order of magnitude sense. The following examples exhibit an accuracy better than within a factor of 2 or 1/2. The analysis is based on the complete problem statement, that is, the conservation equations and all the initial and boundary conditions. Partial differential equations are replaced by global algebraic statements, which are approximate. Scale analysis is a problem-solving method—a method of solution that should not be confused with dimensional analysis.

A simple class of flows that can be described based on scale analysis is boundary layers. Figure 2.1 shows the thermal boundary layer in the vicinity of an isothermal solid wall (T_0) embedded in a saturated porous medium

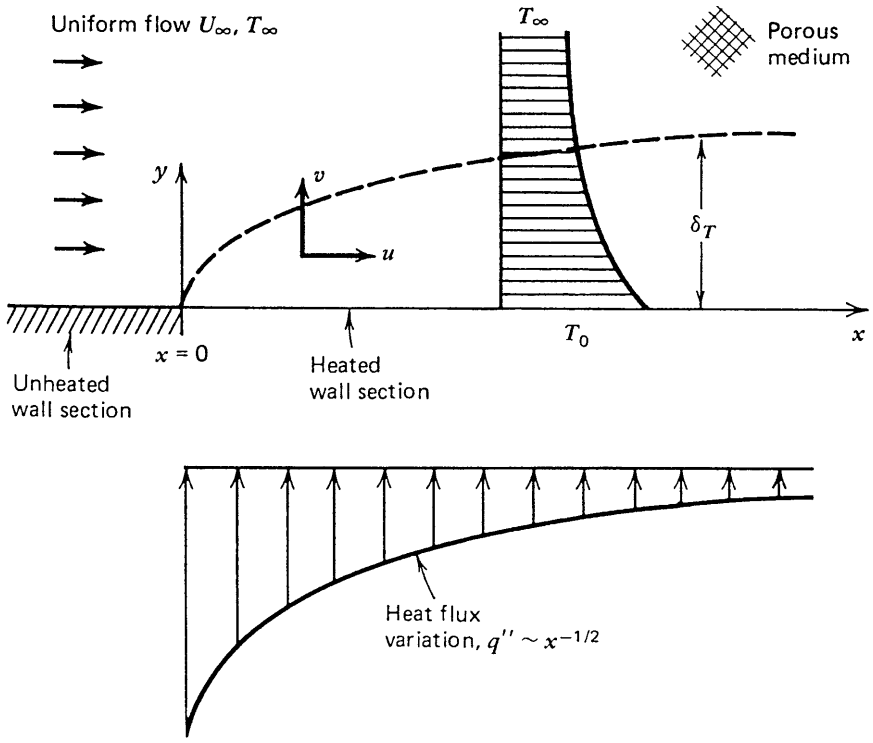

Fig. 2.1. Thermal boundary layer near an isothermal wall with parallel flow.

with uniform flow parallel to the wall (U_∞, T_∞). For simplicity, we assume temperature-independent properties, so that the temperature field is independent of the flow field. The flow field is known: it is the uniform flow U_∞, which in Darcy or Darcy–Forchheimer flow (cf. Section 1.3) is driven by a uniform and constant pressure gradient (dP/dx). Unknown are the temperature distribution in the vicinity of the wall and the heat transfer between the wall and the porous medium.

The analysis refers to the boundary layer regime, which is based on the assumption that the region in which the thermal effect of the wall is felt is *slender*,

$$\delta_T \ll x. \tag{2.1}$$

The boundary layer region has the length x and thickness δ_T. The latter is defined as the distance y where the temperature is practically the same as the approaching temperature (T_∞), or where $\partial T/\partial y \cong 0$. The thermal boundary layer thickness δ_T is the unknown geometric feature that is also the solution to the heat transfer problem. The wall heat flux is given by

$$q'' = k\left(-\frac{\partial T}{\partial y}\right)_{y=0}, \tag{2.2}$$

where k is the effective thermal conductivity of the porous medium saturated with fluid. The scale of the temperature gradient appearing in Equation (2.2) is given by

$$\left(-\frac{\partial T}{\partial y}\right)_{y=0} \sim -\frac{T_\infty - T_0}{\delta_T - 0} = \frac{\Delta T}{\delta_T}, \tag{2.3}$$

where ΔT is the overall temperature difference that drives q''. In conclusion, the heat flux scale is given by

$$q'' \sim k\frac{\Delta T}{\delta_T}, \tag{2.4}$$

which means that in order to estimate q'' we must first estimate δ_T.

The required equation for δ_T is provided by the energy equation, namely, Equation (1.32),

$$u\frac{\partial T}{\partial x} + v\frac{\partial T}{\partial y} = \alpha\frac{\partial^2 T}{\partial y^2}, \tag{2.5}$$

where $\alpha = k/(\rho c_p)_f$ is the thermal diffusivity of the saturated porous medium. The volume-averaged velocity components of the uniform flow are $u = U_\infty$ and $v = 0$, such that Equation (2.5) becomes

$$U_\infty\frac{\partial T}{\partial x} = \alpha\frac{\partial^2 T}{\partial y^2}. \tag{2.6}$$

To determine the order of magnitude of $\partial^2 T/\partial y^2$, we use the same technique as in Equation (2.3): we evaluate the change in $\partial T/\partial y$ from $y = 0$ to $y \sim \delta_T$,

$$\frac{\partial^2 T}{\partial y^2} = \frac{\partial}{\partial y}\left(\frac{\partial T}{\partial y}\right) \sim \frac{(\partial T/\partial y)_{\delta_T} - (\partial T/\partial y)_0}{\delta_T - 0} = \frac{0 + \Delta T/\delta_T}{\delta_T} = \frac{\Delta T}{\delta_T^2}. \quad (2.7)$$

Similarly, for $\partial T/\partial x$ we look at the change in T along the system, from $x = 0$ to x, at a constant y sufficiently close to the wall:

$$\frac{\partial T}{\partial x} \sim \frac{(T)_x - (T)_{x=0}}{x - 0} = \frac{T_0 - T_\infty}{x} = \frac{\Delta T}{x}. \quad (2.8)$$

Together, Equations (2.6) to (2.8) produce

$$U_\infty \frac{\Delta T}{x} \sim \alpha \frac{\Delta T}{\delta_T^2}, \quad (2.9)$$

which is the approximate algebraic statement that replaces the partial differential Equation (2.6). The boundary layer thickness follows from Equation (2.9),

$$\delta_T \sim \left(\frac{\alpha x}{U_\infty}\right)^{1/2} \quad (2.10)$$

and so does the conclusion that δ_T increases as $x^{1/2}$, as shown in Figure 2.1. The heat flux decreases as $x^{-1/2}$, [cf. Equation (2.4)],

$$q'' \sim k\Delta T \left(\frac{U_\infty}{\alpha x}\right)^{1/2}. \quad (2.11)$$

The dimensionless version of this heat transfer rate is given by

$$\mathrm{Nu}_x \sim \mathrm{Pe}_x^{1/2}, \quad (2.12)$$

where the Nusselt and Péclet numbers are given by

$$\mathrm{Nu}_x = \frac{q'' x}{k\Delta T} \qquad \mathrm{Pe}_x = \frac{U_\infty x}{\alpha}. \quad (2.13)$$

These estimates are valid when the heart of boundary layer theory, the slenderness assumption (1), is respected, and this translates into the requirement that $\mathrm{Pe}_x \gg 1$, or that U_∞ and/or x must be sufficiently large.

How approximate is this heat transfer solution? The exact solution to the same thermal boundary layer problem is available in closed form, after solving Equation (2.6) in similarity formulation. The details of this analysis may be found in Bejan (1995a). The similarity solution for the local heat flux is given by

$$\mathrm{Nu}_x = 0.564\mathrm{Pe}_x^{1/2}. \quad (2.14)$$

This agrees with the scaling estimate (2.12). The heat flux averaged over a wall of length L,

$$\overline{q''} = \frac{1}{L}\int_0^L q''\,dx \tag{2.15}$$

can be estimated based on Equation (2.14),

$$\overline{\mathrm{Nu}} = 1.128\mathrm{Pe}_L, \tag{2.16}$$

where corresponding Nusselt and Péclet number definitions are given by

$$\overline{\mathrm{Nu}} = \frac{\overline{q''}L}{k\Delta T}, \qquad \mathrm{Pe}_L = \frac{U_\infty L}{\alpha}. \tag{2.17}$$

Equation (2.16) shows that the scaling estimate (2.12) is again accurate within a factor of order 1. Furthermore, scale analysis makes no distinction between local flux and wall-averaged heat flux: both have the same scale, and the correct scale is delivered by scale analysis, Equation (2.11).

The analysis that produced Equation (2.11) did not require the wall temperature be uniform, $\Delta T = \text{constant}$. We made this assumption only later, when we formulated Nu_x and $\overline{\mathrm{Nu}}$. Equation (2.11) is the general and correct relation between the heat flux scale (q'') and wall excess temperature scale (ΔT) in the boundary layer configuration. Equation (2.11) can be used in situations other than the isothermal-wall case of Figure 2.1. For example, when the wall heat flux is uniform, Equation (2.11) delivers the scale and character of the wall temperature distribution, $\Delta T = T_0(x) - T_\infty$. In local Nusselt number formulation, the scaling result is

$$\mathrm{Nu}_x = \frac{q''x}{k[T_0(x) - T_\infty]} \sim \mathrm{Pe}_x^{1/2}. \tag{2.18}$$

The corresponding local and overall Nusselt numbers derived from the similarity solution to the same problem are

$$\mathrm{Nu}_x = \frac{q''x}{k[T_0(x) - T_\infty]} = 0.886\mathrm{Pe}_x^{1/2} \tag{2.19}$$

$$\overline{\mathrm{Nu}} = \frac{q''L}{k(\bar{T} - T_\infty)} = 1.329\mathrm{Pe}_L^{1/2}, \tag{2.20}$$

where $\bar{T}$ is $T(x)$ averaged from $x = 0$ to $x = L$. Once again, the scaling result (2.18) anticipates within 12 and 33% the similarity solution, Equations (2.19) and (2.20). The trends are identical, and correct. To appreciate how simple, direct, and cost effective scale analysis is, the reader should try to solve the problems using other methods.

2.3 Sphere and Cylinder with Forced Convection

We continue with several examples of forced convection around other bodies embedded in porous media. Figure 2.2a shows the thermal boundary layer region around a sphere, or around a circular cylinder that is perpendicular to a uniform flow with volume averaged velocity u. The sphere or cylinder radius is r_0, and the surface temperature is T_w. The distributions of heat flux around the sphere and cylinder in Darcy flow were determined in Cheng (1982). With reference to the angular coordinate θ, the local peripheral Nusselt numbers for the sphere are

$$\mathrm{Nu}_\theta = 0.564 \left(\frac{ur_0\theta}{\alpha}\right)^{1/2} \left(\frac{3}{2}\theta\right)^{1/2} \sin^2\theta \left(\frac{1}{3}\cos^3\theta - \cos\theta + \frac{2}{3}\right)^{-1/2} \tag{2.21}$$

and for the cylinder:

$$\mathrm{Nu}_\theta = 0.564 \left(\frac{ur_0\theta}{\alpha}\right)^{1/2} (2\theta)^{1/2} \sin\theta\,(1-\cos\theta)^{-1/2}. \tag{2.22}$$

The Péclet number is based on the swept arc $r_0\theta$, namely, $\mathrm{Pe}_\theta = ur_0\theta/\alpha$. The local Nusselt number is defined as

$$\mathrm{Nu}_\theta = \frac{q''}{T_w - T_\infty}\frac{r_0\theta}{k}. \tag{2.23}$$

Equations (2.21) and (2.22) are valid when the boundary layers are distinct (thin), that is, when the boundary layer thickness $r_0\mathrm{Pe}_\theta^{-1/2}$ is smaller than the radius r_0. This requirement can also be written as $\mathrm{Pe}_\theta^{1/2} \gg 1$, or $\mathrm{Nu}_\theta \gg 1$.

The analogy between the thermal boundary layers of the cylinder and the sphere (Figure 2.2a) and that of the flat wall (Figure 2.1) is illustrated further by Nield and Bejan's (1999) correlation of the heat transfer results for these

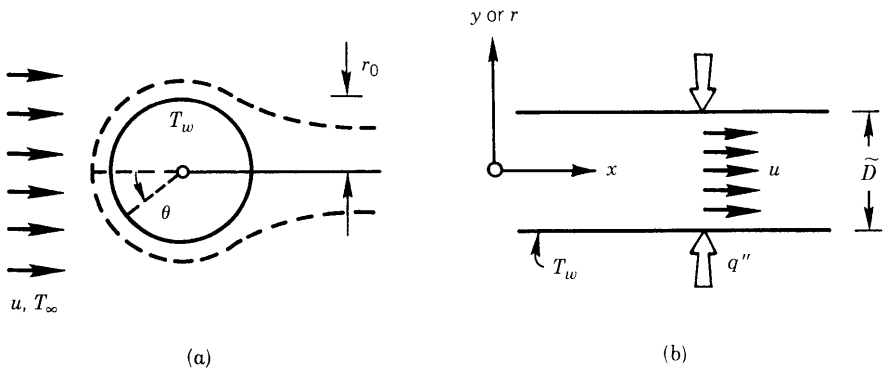

Fig. 2.2. Forced convection in porous media: (a) boundary layer around a sphere or cylinder; (b) channel filled with a porous medium.

three configurations. The heat flux averaged over the area of the cylinder and sphere, $\bar{q}''$, can be calculated by averaging the local heat flux q'' expressed by Equations (2.21) through (2.23). The results for the sphere are

$$\overline{\mathrm{Nu}}_D = 1.128\mathrm{Pe}_D^{1/2} \tag{2.24}$$

and for the cylinder

$$\overline{\mathrm{Nu}}_D = 1.015\mathrm{Pe}_D^{1/2}. \tag{2.25}$$

In these expressions, the Nusselt and Péclet numbers are based on the diameter $D = 2r_0$,

$$\overline{\mathrm{Nu}}_D = \frac{\overline{q''}D}{(T_w - T_\infty)k}, \qquad \mathrm{Pe}_D = \frac{uD}{\alpha}. \tag{2.26}$$

In summary, the overall Nusselt number is nearly equal to $\mathrm{Pe}_D^{1/2}$, in accordance with the scale analysis presented in Section 2.2. The purpose of the present section was to review the exact results that are available for the sphere and cylinder, and to direct the reader to the appropriate sources in the literature.

2.4 Channels with Porous Media and Forced Convection

Consider now the forced convection heat transfer in a channel or duct packed with a uniform and isotropic porous material as in Figure 2.2b. In the Darcy flow regime the longitudinal volume-averaged velocity u is uniform over the channel cross-section. When the temperature field is fully developed, the relationship between the wall heat flux q'' and the local temperature difference $(T_w - T_b)$ is analogous to the relationship for fully developed heat transfer to slug flow through a channel without a porous matrix (Bejan, 1995a). The temperature T_b is the mean or bulk temperature of the stream that flows through the channel,

$$T_b = \frac{1}{A}\int_A T\,dA, \tag{2.27}$$

in which A is the area of the channel cross-section. In general, when the velocity u is not uniform over the channel cross-section, T_b is weighted with the velocity,

$$T_b = \frac{1}{\bar{u}A}\int_A uT\,dA, \tag{2.27'}$$

where $\bar{u}$ is the velocity averaged over A. In cases where the confining wall is a tube with internal diameter D, the relation for fully developed heat transfer can be expressed as a constant Nusselt number (Rohsenow and Choi, 1961):

$$\mathrm{Nu}_D = \frac{q''(x)}{T_w - T_b(x)}\frac{D}{k} = 5.78 \quad (\text{tube}, T_w = \text{uniform}), \tag{2.28}$$

$$\mathrm{Nu}_D = \frac{q''}{T_w(x) - T_b(x)}\frac{D}{k} = 8 \quad (\text{tube}, q'' = \text{uniform}). \tag{2.29}$$

When the porous matrix is sandwiched between two parallel plates with the spacing D, the corresponding Nusselt numbers are (Rohsenow and Hartnett, 1973)

$$\mathrm{Nu}_D = \frac{q''(x)}{T_w - T_b(x)}\frac{D}{k} = 4.93 \quad \text{(parallel plates, } T_w = \text{uniform)}, \quad (2.30)$$

$$\mathrm{Nu}_D = \frac{q''}{T_w(x) - T_b(x)}\frac{D}{k} = 6 \quad \text{(parallel plates, } q'' = \text{uniform)}. \quad (2.31)$$

The forced convection results of Equations (2.28) through (2.31) are valid when the temperature profile across the channel is fully developed (sufficiently far from the entrance $x = 0$). The entrance length, or the length needed for the temperature profile to become fully developed, can be estimated by noting that the thermal boundary layer thickness scales as $(\alpha x/u)^{1/2}$. Setting $(\alpha x/u)^{1/2} \sim D$, the thermal entrance length $x_T \sim D^2 u/\alpha$ is obtained. Inside the entrance region $0 < x < x_T$, the heat transfer is impeded by the forced convection thermal boundary layers that line the channel walls, and can be calculated approximately using the results of Section 2.2.

One important application of the results for a channel packed with a porous material is in the area of heat transfer augmentation. As shown by Nield and Bejan (1999), the Nusselt numbers for fully developed heat transfer in a channel without a porous matrix are given by expressions similar to Equations (2.28) through (2.31) except that the saturated porous medium conductivity k is replaced by the thermal conductivity of the fluid alone, k_f. The relative heat transfer augmentation effect is indicated approximately by the ratio

$$\frac{h_x(\text{with porous matrix})}{h_x(\text{without porous matrix})} \sim \frac{k}{k_f} \quad (2.32)$$

in which h_x is the local heat transfer coefficient $q''/(T_w - T_b)$. In conclusion, a significant heat transfer augmentation effect can be achieved by using a high-conductivity matrix material, so that k is considerably greater than k_f. This effect is accompanied by a significant increase in fluid flow resistance.

Key results for forced convection in porous media have been developed based on constructal theory for tree networks of cracks (Bejan, 2000), time-dependent heating, annular channels, stepwise changes in wall temperature, local thermal nonequilibrium, and other external flows (such as over a cone or wedge). The concepts of heatfunctions and heatlines were introduced for the purpose of visualizing the true path of the flow of energy through a convective medium (Bejan, 1984, 1995a). The heatfunction accounts simultaneously for the transfer of heat by conduction and convection at every point in the medium. The heatlines are a generalization of the flux lines used routinely in the field of conduction. The concept of heatfunction is a spatial generalization of the concept of the Nusselt number, that is, a way of indicating the magnitude of the heat transfer rate through any unit surface drawn through any point on the convective medium. The heatline method was extended to several configurations of convection through fluid saturated porous media (Morega and Bejan, 1994).

2.5 Scale Analysis of Natural Convection Boundary Layers

We return to the method of scale analysis, and consider the natural convection boundary layer near a vertical impermeable wall embedded in a saturated porous medium at a different temperature. The boundary conditions are indicated in Figure 2.3, where the gravitational acceleration points in the negative y-direction. The equations for mass conservation and Darcy flow,

$$\frac{\partial u}{\partial x} + \frac{\partial v}{\partial y} = 0, \tag{2.33}$$

$$u = -\frac{K}{\mu}\frac{\partial P}{\partial x}, \qquad v = -\frac{K}{\mu}\left(\frac{\partial P}{\partial y} + \rho g\right), \tag{2.34}$$

can be rewritten as a single equation

$$\frac{\partial^2 \psi}{\partial x^2} + \frac{\partial^2 \psi}{\partial y^2} = -\frac{Kg\beta}{\nu}\frac{\partial T}{\partial x}, \tag{2.35}$$

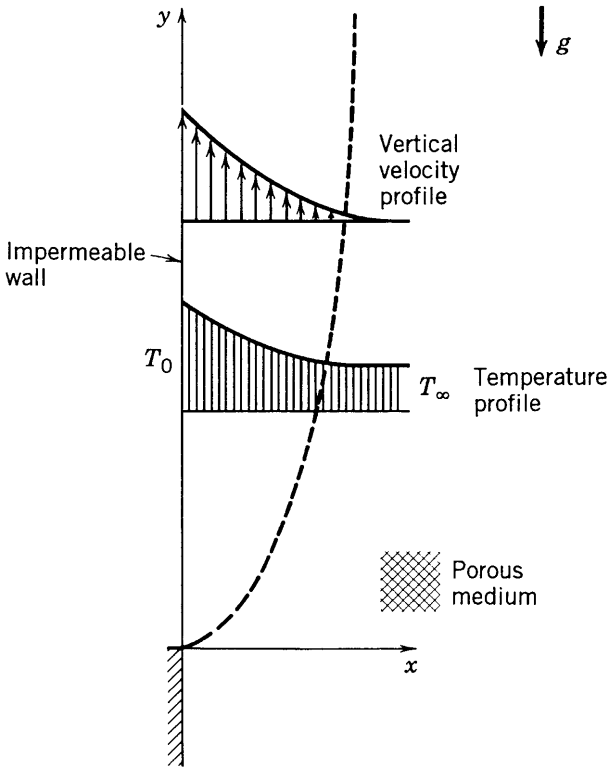

Fig. 2.3. Natural convection boundary layer near a heated vertical impermeable wall.

where $\psi(x, y)$ is the streamfunction for volume-averaged flow, $u = \partial\psi/\partial y$ and $v = -\partial\psi/\partial x$. In Equation (2.35) we used the Boussinesq approximation $\rho = \rho_0[1 - \beta(T - T_0)]$, which effects the coupling of the velocity field to the temperature field. The energy conservation equation for boundary layer flow is given by [cf. Equation (2.5)]

$$\frac{\partial\psi}{\partial y}\frac{\partial T}{\partial x} - \frac{\partial\psi}{\partial x}\frac{\partial T}{\partial y} = \alpha\frac{\partial^2 T}{\partial x^2}. \tag{2.36}$$

The problem is to determine the heat transfer rate between the wall and the medium, $q'' \sim k\Delta T/\delta_T$, where $\Delta T = T_0 - T_\infty$, and δ_T is the thickness of the boundary layer region ($\delta_T \ll y$). By invoking the temperature boundary conditions sketched in Figure 2.3, and using the rules of scale analysis outlined in Section 2.2, we find that the terms of Equations (2.35) and (2.36) are represented by the following scales,

$$\frac{\psi}{\delta_T^2}, \quad \frac{\psi}{y^2} \sim \frac{Kg\beta\Delta T}{\nu\delta_T}, \tag{2.37}$$

$$\frac{\psi\Delta T}{y\delta_T}, \quad \frac{\psi\Delta T}{\delta_T y} \sim \alpha\frac{\Delta T}{\delta_T^2}. \tag{2.38}$$

On the left side of Equation (2.37) we retain the first scale, because $\psi/\delta_T^2 > \psi/y^2$. On the left side of Equation (2.38), the two scales are represented by the same order of magnitude, $\psi\Delta T/(y\delta_T)$. Together, Equations (2.37) and (2.38) are sufficient for determining the two unknown scales, δ_T and ψ,

$$\frac{\delta_T}{y} \sim \mathrm{Ra}_y^{-1/2}, \qquad \psi \sim \alpha\mathrm{Ra}_y^{1/2}, \tag{2.39}$$

where Ra_y is the Darcy-modified Rayleigh number, $\mathrm{Ra}_y = Kg\beta y\,\Delta T/(\alpha\nu)$. From the ψ scale we conclude that the vertical velocity scale is $v \sim \psi/\delta_T$, or $v \sim (\alpha/y)\mathrm{Ra}_y \sim Kg\beta\,\Delta T/\nu$. From the δ_T scale we deduce the heat flux, or the Nusselt number,

$$\mathrm{Nu}_y = \frac{q''y}{k\Delta T} \sim \mathrm{Ra}_y^{1/2}. \tag{2.40}$$

This scale agrees with the similarity solution to the problem of the boundary layer along an isothermal wall of temperature T_0 (Cheng and Minkowycz, 1977),

$$\mathrm{Nu}_y = \frac{q''y}{(T_0 - T_\infty)k} = 0.444\mathrm{Ra}_y^{1/2}, \tag{2.41}$$

$$\overline{\mathrm{Nu}} = \frac{\overline{q''}H}{(T_0 - T_\infty)k} = 0.888\mathrm{Ra}_H^{1/2}. \tag{2.42}$$

If the wall has uniform heat flux, then the local wall temperature and the boundary layer thickness must vary such that

$$q'' \sim k\frac{T_0(y)-T_\infty}{\delta_T} = \text{constant}. \tag{2.43}$$

Combining this with the δ_T scale (2.39), we conclude that

$$\frac{\delta_T}{y} \sim \text{Ra}_{*y}^{-1/3}, \tag{2.44}$$

where Ra_{*y} is the Darcy-modified Rayleigh number based on heat flux, $\text{Ra}_{*y} = Kg\beta y^2 q''/(\alpha\nu k)$. The local heat transfer rate must therefore scale as

$$\text{Nu}_y = \frac{q''}{T_0(y)-T_\infty}\frac{y}{k} \sim \text{Ra}_{*y}^{1/3}. \tag{2.45}$$

The numerical solution to the similarity for formulation of this problem is given by (Bejan, 1995a)

$$\text{Nu}_y = \frac{q''}{T_0(y)-T_\infty}\frac{y}{k} = 0.772\text{Ra}_{*y}^{1/3}, \tag{2.46}$$

$$\overline{\text{Nu}} = \frac{q''}{\overline{T}_0-T_\infty}\frac{H}{k} = 1.03\text{Ra}_{*H}^{1/3}, \tag{2.47}$$

where H is the wall height. In conclusion, Equations (2.45) to (2.47) show that the exact results are anticipated within 23% by the results of scale analysis. More examples of boundary layer natural convection in porous media are reviewed in the next section.

2.6 Thermal Stratification and Vertical Partitions

When the porous medium of Figure 2.3 is finite in the x- and y-directions, the discharge of the heated vertical stream into the rest of the medium leads in time to thermal stratification. This problem was considered in Bejan (1984). As shown in Figure 2.4, the original wall excess temperature is $T_0 - T_{\infty,0}$, and the porous medium is stratified according to the positive vertical gradient $\gamma = dT_\infty/dy$. The local temperature difference $T_0 - T_\infty(y)$ decreases as y increases, which is why a monotonic decrease in the total heat transfer rate as γ increases should be expected. This trend is confirmed by the right-hand part of the figure, which shows the integral solution developed for this configuration. The overall Nusselt number, Rayleigh number, and stratification parameter are defined as

$$\overline{\text{Nu}}_H = \frac{\overline{q''}H}{k(T_0-T_{\infty,0})}, \qquad \text{Ra}_H = \frac{Kg\beta H}{\alpha\nu}(T_0-T_{\infty,0}), \qquad b = \frac{\gamma H}{T_0-T_{\infty,0}}. \tag{2.48}$$

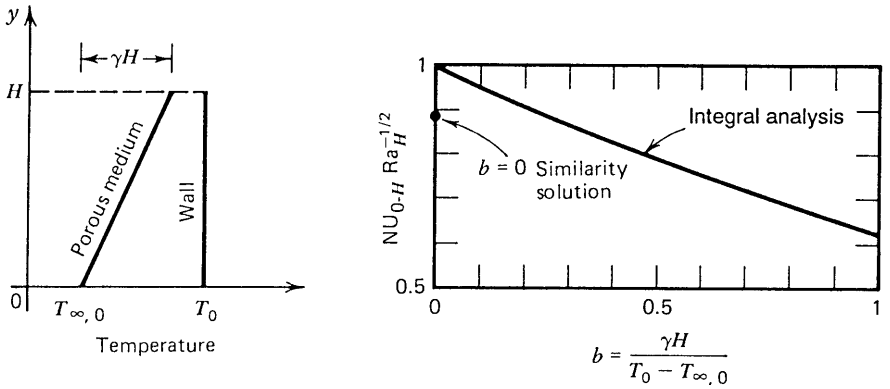

Fig. 2.4. Heat transfer solution for a vertical isothermal wall facing a linearly stratified porous medium saturated with fluid (Bejan, 1984; from Bejan, *Convection Heat Transfer*, 2nd ed., Copyright © 1995 Wiley. This material is used by permission of John Wiley & Sons, Inc.).

The accuracy of this integral solution can be assessed by comparing its $b = 0$ limit

$$\frac{\overline{\mathrm{Nu}}_H}{\mathrm{Ra}_H^{1/2}} = 1 \qquad (b = 0) \tag{2.49}$$

with the similarity solution for an isothermal wall adjacent to an isothermal porous medium, Equation (2.42). The integral solution overestimates the global heat transfer rate by only 12.6% (Figure 2.4).

The breakdown of the Darcy flow model in vertical boundary layer natural convection was the subject of several studies (Plumb and Huenefeld, 1981; Bejan and Poulikakos, 1984; Nield and Joseph, 1985). Assuming the Dupuit–Forchheimer modification of the Darcy flow model, at local pore Reynolds numbers greater than 10, the local Nusselt number for the vertical wall configuration of Figure 2.3 approaches the following limits (Bejan and Poulikakos, 1984),

$$\mathrm{Nu}_y = 0.494\mathrm{Ra}_{\infty,y}^{1/4} \quad \text{for the isothermal wall,} \tag{2.50}$$

$$\mathrm{Nu}_y = 0.804\mathrm{Ra}_{\infty,y}^{*1/5} \quad \text{for the constant heat flux wall,} \tag{2.51}$$

where $\mathrm{Ra}_{\infty,y} = g\beta y^2(T_w - T_\infty)/(b\alpha^2)$ and $\mathrm{Ra}^*_{\infty,y} = g\beta y^3 q''/(kb\alpha^2)$, and $b[m^{-1}]$ is defined in Equation (1.12). Equations (2.50) and (2.51) are valid provided $G \ll 1$, where $G = (\nu/K)[bg\beta(T_w - T_\infty)]^{-1/2}$. In the intermediate range between the Darcy limit and the inertia-dominated limit (or form drag limit), that is, in the range where G is of order one, numerical results for a vertical isothermal wall (Bejan and Poulikakos, 1984) are correlated within 2% by the closed-form expression (Bejan, 1987)

$$\mathrm{Nu}_y = [(0.494)^n + (0.444G^{-1/2})^n]^{1/n}\mathrm{Ra}_{\infty,y}^{1/4}, \tag{2.52}$$

where $n = -3$. The heat transfer results summarized in this section also apply to configurations where the vertical wall is inclined (slightly) to the vertical. In such cases, the gravitational acceleration that appears in the definition of the Rayleigh-type numbers in this section must be replaced by the gravitational acceleration component that acts along the nearly vertical wall.

When a vertical wall divides two porous media, and a temperature difference exists between the two systems, there is a pair of conjugate boundary layers, one on each side of the wall, with neither the temperature nor the heat flux specified on the wall but rather to be found as part of the solution to the problem (Figure 2.5a) (Bejan and Anderson, 1981). The overall Nusselt number results for this configuration are correlated within 1% by the expression

$$\overline{\mathrm{Nu}}_H = 0.382(1 + 0.615\omega)^{-0.875}\mathrm{Ra}_H^{1/2}, \tag{2.53}$$

where $\overline{\mathrm{Nu}}_H = \overline{q''}H/[(T_{\infty,H} - T_{\infty,L})k]$, and where $\overline{q''}$ is the heat flux averaged over the entire height H. In addition, $\mathrm{Ra}_H = Kg\beta H(T_{\infty,H} - T_{\infty,L})/(\alpha\nu)$.

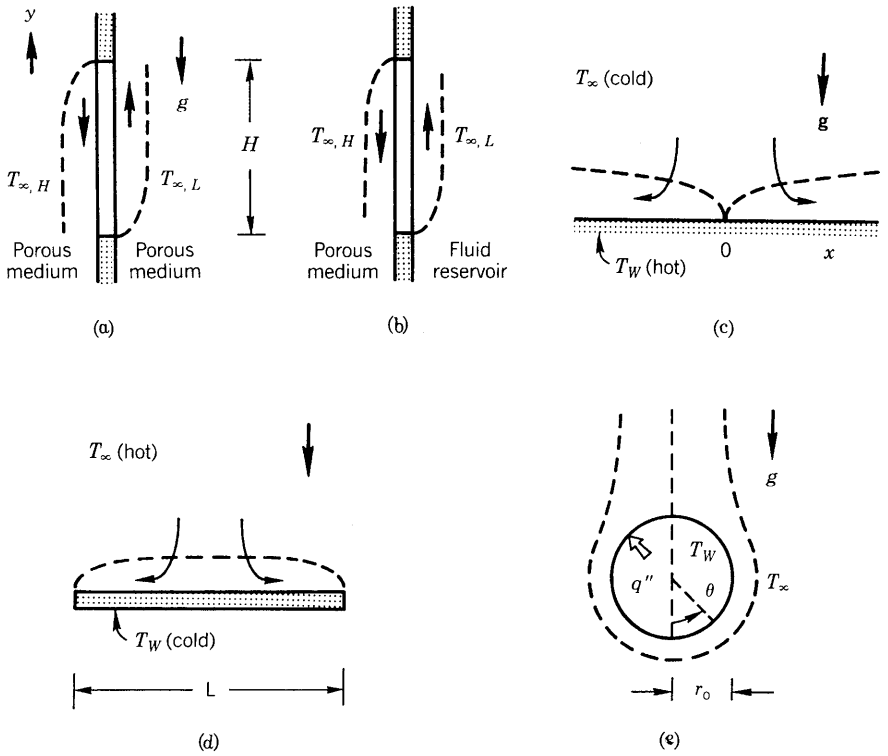

Fig. 2.5. Natural convection boundary layers in porous media: (a) vertical partition with porous media on both sides; (b) vertical wall separating a porous medium and a fluid reservoir; (c) hot surface facing upward; (d) cold surface facing downward; (e) sphere or cylinder embedded in a porous medium.

The wall thickness parameter ω is

$$\omega = \frac{W}{H}\frac{k}{k_w}\mathrm{Ra}_H^{1/2}, \tag{2.54}$$

where W and H are the width and height of the wall cross-section, k and k_w are the conductivities of the porous medium and wall material, respectively, and Ra_H is the Rayleigh number based on H and the temperature difference between the two systems. The progress on conjugate boundary layers was reviewed by Kimura *et al.* (1997).

In thermal insulation and architectural applications, the porous media on both sides of the vertical partition of Figure 2.5a may be thermally stratified. If the stratification on both sides is the same and linear (e.g., Figure 2.4), so that the vertical temperature gradient far enough from the wall is $dT/dy = b_1(T_{\infty,H} - T_{\infty,L})/H$, where b_1 is a constant, and if the partition is thin enough so that $\omega \approx 0$, then it is found that the overall Nusselt number increases substantially with the degree of stratification (Bejan and Anderson, 1983). In the range $0 < b_1 < 1.5$, these findings are summarized by the correlation

$$\overline{\mathrm{Nu}}_H = 0.382(1 + 0.662b_1 - 0.073b_1^2)\mathrm{Ra}_H^{1/2}. \tag{2.55}$$

Another configuration of engineering interest is sketched in Figure 2.5b: a vertical impermeable surface separates a porous medium of temperature $T_{\infty,H}$ from a fluid reservoir of temperature $T_{\infty,L}$ (Bejan and Anderson, 1983). When both sides of the interface are lined by boundary layers, the overall Nusselt number is

$$\overline{\mathrm{Nu}}_H = [(0.638)^{-1} + (0.888B)^{-1}]^{-1}\mathrm{Ra}_{H,f}^{1/4}, \tag{2.56}$$

where $\overline{\mathrm{Nu}}_H = \overline{q''}H/[(T_{\infty,H} - T_{\infty,L})k]$ and $B = k\mathrm{Ra}_H^{1/2}/(k_f\mathrm{Ra}_{H,f}^{1/4})$. The parameter k_f is the fluid-side thermal conductivity, and the fluid-side Rayleigh number $\mathrm{Ra}_{H,f} = g(\beta/\alpha\nu)_f H^3(T_{\infty,H} - T_{\infty,L})$. Equation (2.56) is valid in the regime where both boundary layers are distinct, $\mathrm{Ra}_H^{1/2} \gg 1$ and $\mathrm{Ra}_{H,f}^{1/4} \gg 1$. It is also assumed that the fluid on the right side of the partition in Figure 2.5b has a Prandtl number of order 1 or greater. For a numerical model and simulation of a porous-fluid interface, see Costa *et al.* (2004). Additional solutions for boundary layer convection in the vicinity of vertical partitions in porous media are reviewed in Nield and Bejan (1999). The heat flow near the interface between a porous medium with natural convection and a conducting solid was illustrated with *heatlines* by Costa (2003).

2.7 Horizontal Walls with Natural Convection

With reference to Figure 2.5c, boundary layers form in the vicinity of a heated horizontal surface that faces upward (Cheng and Chang, 1976). Measuring x

horizontally away from the vertical plane of symmetry of the flow, the local Nusselt number for an isothermal wall is

$$\mathrm{Nu}_x = 0.42\mathrm{Ra}_x^{1/3}, \tag{2.57}$$

where $\mathrm{Nu}_x = q''x/[k(T_w - T_\infty)]$ and $\mathrm{Ra}_x = Kg\beta x(T_w - T_\infty)/(\alpha\nu)$. The local Nusselt number for a horizontal wall heated with uniform flux is

$$\mathrm{Nu}_x = 0.859\mathrm{Ra}_x^{*1/4}, \tag{2.58}$$

where $\mathrm{Ra}_x^* = Kg\beta x^2 q''/(k\alpha\nu)$. Equations (2.57) and (2.58) are valid in the boundary layer regime, $\mathrm{Ra}_x^{1/3} \gg 1$ and $\mathrm{Ra}_x^{*1/4} \gg 1$, respectively. They also apply to porous media bounded from above by a cold surface; this new configuration is obtained by rotating Figure 2.5c by 180°.

The upward-facing cold plate of Figure 2.5d was studied in Kimura *et al.* (1985). The overall Nusselt number in this configuration is

$$\mathrm{Nu} = 1.47\mathrm{Ra}_L^{1/3}, \tag{2.59}$$

where $\mathrm{Nu} = q'/[k(T_\infty - T_w)]$ and $\mathrm{Ra}_L = Kg\beta L(T_\infty - T_w)/(\alpha\nu)$, and where q' is the overall heat transfer rate through the upward-facing cold plate of length L. Equation (2.59) holds if $\mathrm{Ra}_L \gg 1$, and applies equally to hot horizontal plates facing downward in an isothermal porous medium. Note the exponent 1/3, which is in contrast to the exponent 1/2 for the vertical wall in Equation (2.42).

2.8 Sphere and Horizontal Cylinder with Natural Convection

With reference to the coordinate system shown in the circular cross-section sketched in Figure 2.5e, the local Nusselt numbers for boundary layer convection around an impermeable sphere or a horizontal cylinder embedded in an infinite porous medium are, in order (Cheng, 1982),

$$\mathrm{Nu}_\theta = 0.444\mathrm{Ra}_\theta^{1/2}\left(\frac{3}{2}\theta\right)^{1/2}\sin^2\theta\left(\frac{1}{3}\cos^3\theta - \cos\theta + \frac{2}{3}\right)^{-1/2}, \tag{2.60}$$

$$\mathrm{Nu}_\theta = 0.444\mathrm{Ra}_\theta^{1/2}(2\theta)^{1/2}\sin\theta(1-\cos\theta)^{-1/2}, \tag{2.61}$$

where $\mathrm{Nu}_\theta = q''r_0\theta/[k(T_w - T_\infty)]$ and $\mathrm{Ra}_\theta = Kg\beta\theta r_0(T_w - T_\infty)/(\alpha\nu)$. These steady-state results are valid provided the boundary layer region is slender enough, that is, if $\mathrm{Nu}_\theta \gg 1$. The overall Nusselt numbers for the sphere and horizontal cylinder are, respectively (Nield and Bejan, 1999),

$$\overline{\mathrm{Nu}}_D = 0.362\mathrm{Ra}_D^{1/2}, \tag{2.62}$$

$$\overline{\mathrm{Nu}}_D = 0.565\mathrm{Ra}_D^{1/2}, \tag{2.63}$$

where $\overline{\mathrm{Nu}}_D = \overline{q''}D/[k(T_w - T_\infty)]$ and $\mathrm{Ra}_D = Kg\beta D(T_w - T_\infty)/(\alpha\nu)$. Solutions for convection at low and intermediate Rayleigh numbers are summarized in Nield and Bejan (1999).

In the review conducted in this chapter we considered separately the fundamentals of forced convection and natural convection. There are many practical situations in which these two flow mechanisms occur together. The resulting class of flows is called mixed convection, and is reviewed in Nield and Bejan (1999). A recent study of mixed convection was performed by Magyari *et al.* (2001). There are many other effects that complicate the modeling of convection in porous media. The effect of a magnetic field and heat generation was considered by Chamkha and Quadri (2001). The modeling of coupled heat and mass transfer was discussed by Mendes *et al.* (2002). Dissipation effects were discussed by Nield (2000).

2.9 Enclosures Heated from the Side

The most basic configuration of a porous layer heated in the horizontal direction is sketched in Figure 2.6. In Darcy flow, the heat and fluid flow driven by buoyancy depend on two parameters: the geometric aspect ratio H/L, and the Rayleigh number based on height, $\mathrm{Ra}_H = Kg\beta H(T_h - T_c)/(\alpha\nu)$. There exist four heat transfer regimes (Bejan, 1984, 1995a), that is, four ways to calculate the overall heat transfer rate $q' = \int_0^H q''dy$. These are summarized in Figure 2.6:

Regime I. The pure conduction regime, defined by $\mathrm{Ra}_H \ll 1$. In this regime, q' is approximately equal to the pure conduction estimate $kH(T_h - T_c)/L$.

Regime II. The conduction-dominated regime in tall layers, defined by $H/L \gg 1$ and $(L/H)\mathrm{Ra}_H^{1/2} \ll 1$. In this regime, the heat transfer rate scales as $q' \geq kH(T_h - T_c)/L$.

Regime III. The convection-dominated regime (or high Rayleigh number regime), defined by $\mathrm{Ra}_H^{-1/2} < H/L < \mathrm{Ra}_H^{1/2}$. In this regime, q' scales as $k(T_h - T_c)\mathrm{Ra}_H^{1/2}$.

Regime IV. The convection-dominated regime in shallow layers, defined by $H/L \ll 1$ and $(H/L)\mathrm{Ra}_H^{1/2} \ll 1$. Here the heat transfer rate scales as $q \leq k(T_h - T_c)\mathrm{Ra}_H^{1/2}$.

Considerable analytical, numerical, and experimental work has been done to estimate more accurately the overall heat transfer rate q' or the overall Nusselt number,

$$\mathrm{Nu} = \frac{q'}{kH(T_h - T_c)/L}. \tag{2.64}$$

Note that unlike the single-wall configuration of Section 2.5, in confined layers of thickness L the Nusselt number is defined as the ratio of the actual heat transfer rate to the pure conduction heat transfer rate. An analytical solution

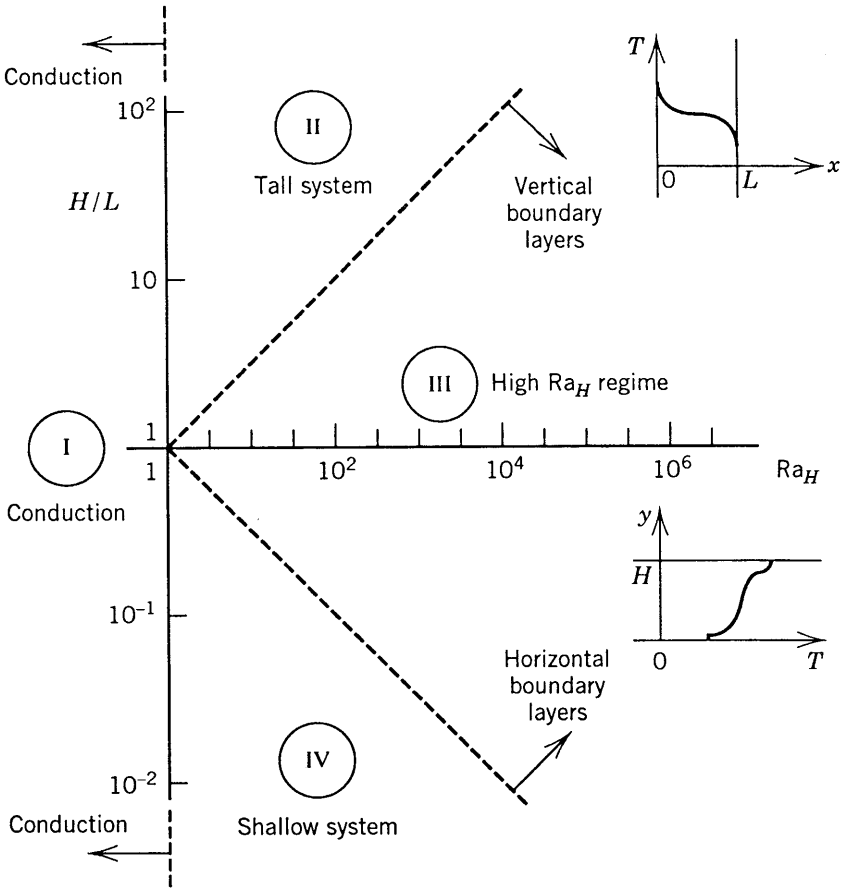

Fig. 2.6. Four heat transfer regimes for natural convection in an enclosed rectangular porous layer heated from the side (Bejan, 1984; from Bejan, *Convection Heat Transfer*, 2nd ed., Copyright © 1995 Wiley. This material is used by permission of John Wiley & Sons, Inc.).

that covers the four heat transfer regimes smoothly is (Bejan and Tien, 1978)

$$\mathrm{Nu} = K_1 + \frac{1}{120} K_1^3 \left(\mathrm{Ra}_H \frac{H}{L} \right)^2, \tag{2.65}$$

where $K_1(H/L, \mathrm{Ra}_H)$ is obtained by solving the system

$$\frac{1}{120} \delta_e \mathrm{Ra}_H^2 K_1^3 \left(\frac{H}{L} \right)^3 = 1 - K_1 = \frac{1}{2} K_1 \frac{H}{L} \left(\frac{1}{\delta_e} - \delta_e \right). \tag{2.66}$$

This result is displayed in chart form in Figure 2.7 along with numerical results from Hickox and Gartling (1981). The asymptotic values of this solution are

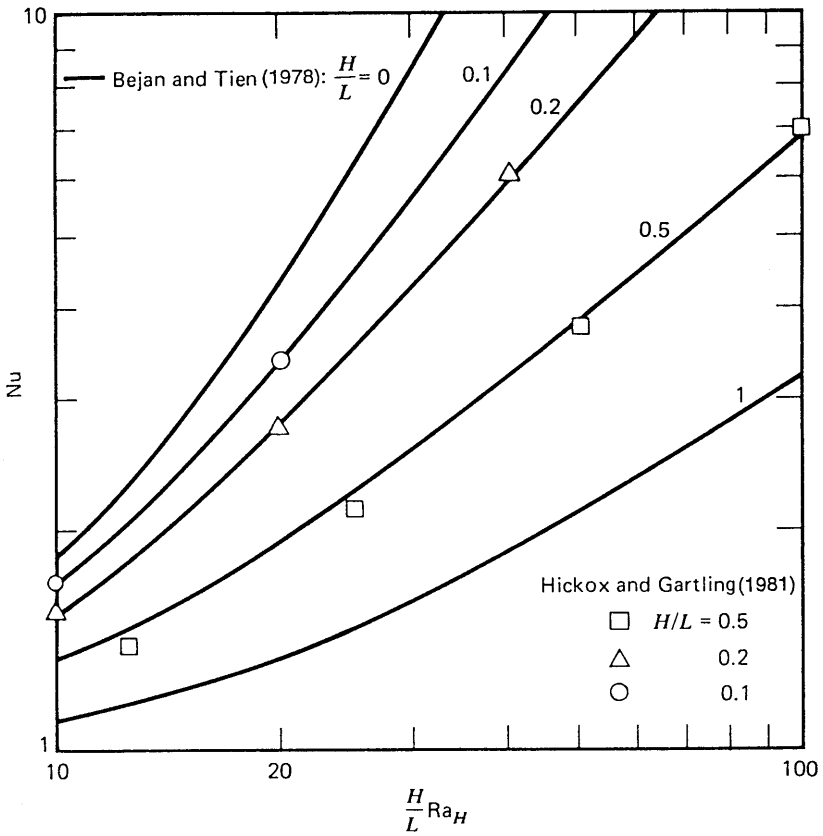

Fig. 2.7. The total heat transfer rate through an enclosed porous layer heated from the side (Bejan and Tien, 1978).

$$\mathrm{Nu} \sim 0.508 \frac{L}{H} \mathrm{Ra}_H^{1/2} \quad \text{as } \mathrm{Ra}_H \to \infty \tag{2.67}$$

$$\mathrm{Nu} \sim 1 + \frac{1}{120} \left(\mathrm{Ra}_H \frac{H}{L} \right)^2 \quad \text{as } \frac{H}{L} \to 0. \tag{2.68}$$

The heat transfer in the convection-dominated Regime III is well represented by Equation (2.67) or by alternate solutions developed solely for Regime III, for example (Weber, 1975), $\mathrm{Nu} = 0.577(L/H)\mathrm{Ra}_H^{1/2}$. More refined estimates for Regime III were developed in Bejan (1979a) and Simpkins and Blythe (1980), where the proportionality factor between Nu and $(L/H)\mathrm{Ra}_H^{1/2}$ is replaced by a function of both H/L and Ra_H; see Figure 2.8. For expedient engineering calculations of heat transfer dominated by convection, Figure 2.7 is recommended for shallow layers ($H/L < 1$), and Figure 2.8 for square and tall layers ($H/L \gtrsim 1$) in the boundary layer regime, $\mathrm{Ra}_H^{-1/2} < H/L < \mathrm{Ra}_H^{1/2}$.

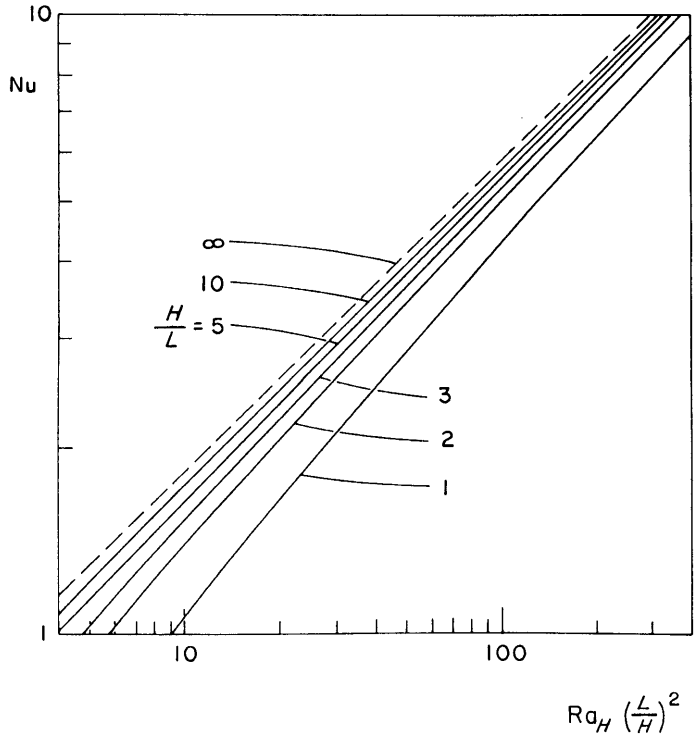

Fig. 2.8. The heat transfer rate in Regime III through a porous layer heated from the side (Bejan, 1979a).

In the field of thermal insulation engineering, a more appropriate model for heat transfer in the configuration of Figure 2.6 is the case where the heat flux q'' is distributed uniformly along the two vertical sides of the porous layer. In the high Rayleigh number regime (Regime III), the overall heat transfer rate is given by (Bejan, 1983a)

$$\mathrm{Nu} = \frac{1}{2}\left(\frac{L}{H}\right)^{4/5} \mathrm{Ra}_H^{*2/5}, \tag{2.69}$$

where $\mathrm{Ra}_H^* = Kg\beta H^2 q''/(\alpha\nu k)$. The overall Nusselt number is defined as in Equation (2.64), where $T_h - T_c$ is the height-averaged temperature difference between the two sides of the rectangular cross-section. Equation (2.69) holds in the high Rayleigh number regime $\mathrm{Ra}_H^{*-1/3} < H/L < \mathrm{Ra}_H^{*1/3}$.

The progress reviewed so far is based on models that assume local thermal equilibrium. Natural convection without local thermal equilibrium was studied based on a two-temperature model by Rees and Pop (2000).

Impermeable partitions (flow obstructions) inserted in the confined porous medium can have a dramatic effect on the overall heat transfer rate across the

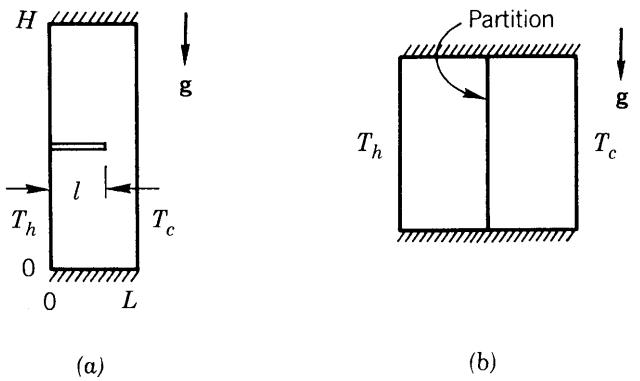

Fig. 2.9. Rectangular enclosure filled with porous medium: (a) partial horizontal partition; (b) full vertical partition.

enclosure (Bejan, 1983b). With reference to the two-dimensional geometry of Figure 2.9a, in the convection-dominated Regimes III and IV the overall heat transfer rate decreases steadily as the length l of the horizontal partition approaches L, that is, as the partition divides the porous layer into two shorter layers. The horizontal partition has practically no effect in Regimes I and II where the overall heat transfer rate is dominated by conduction. If the partition is oriented vertically (Figure 2.9b), then in the convection-dominated regime the overall heat transfer rate is approximately 40% of what it would have been in the same porous medium without the internal partition.

The nonuniformity of permeability and thermal diffusivity can have a dominating effect on the overall heat transfer rate (Poulikakos and Bejan, 1983a). In cases where the properties vary so that the porous layer can be modeled as a sandwich of vertical sublayers of different permeability and diffusivity (Figure 2.10a), an important parameter is the ratio of the peripheral sublayer thickness (d_1) to the thermal boundary-layer thickness ($\delta_{T,1}$) based on the

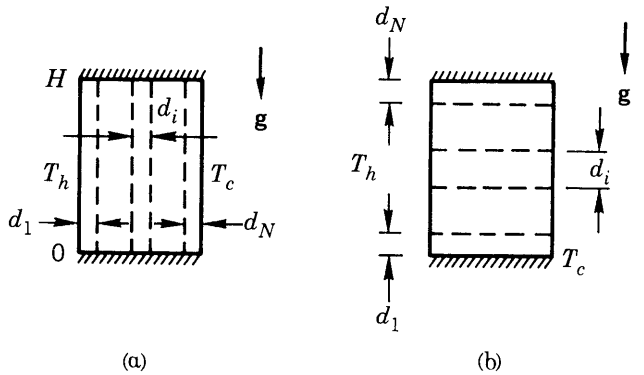

Fig. 2.10. Rectangular enclosure filled with several porous layers: (a) vertical layers; (b) horizontal layers.

properties of the d_1 sublayer (note that $\delta_{T,1}$ scales as $H\,\mathrm{Ra}_{H,1}^{-1/2}$, where the Rayleigh number $\mathrm{Ra}_{H,1} = K_1 g\beta H(T_h - T_c)/(\alpha_1\nu)$ and where the subscript l represents the properties of the d_1 sublayer). If $d_1 > \delta_{T,1}$, then the heat transfer through the left side of the porous system of Figure 2.10a is impeded by a thermal resistance of order $\delta_{T,1}/(k_1 H)$. If the sublayer situated next to the right wall (d_N) has exactly the same properties as the d_1 sublayer, and if $\delta_{T,1} < (d_1, d_N)$, then the overall heat transfer rate in the convection-dominated regime can be estimated using Equation (2.67) in which both Nu and Ra_H are based on the properties of the peripheral layers.

When the porous-medium inhomogeneity may be modeled as a sandwich of N horizontal sublayers (Figure 2.10b), the scale of the overall Nusselt number in the convection-dominated regime can be evaluated as (Poulikakos and Bejan, 1983a)

$$\mathrm{Nu} \sim 2^{-3/2}\mathrm{Ra}_{H,1}^{1/2}\frac{L}{H}\sum_{i=1}^{N}\frac{k_i}{k_1}\left(\frac{K_i d_i \alpha_1}{K_1 d_1 \alpha_i}\right)^{1/2}, \tag{2.70}$$

where both Nu and $\mathrm{Ra}_{H,1}$ are based on the properties of the d_1 sublayer (Figure 2.10b). The correlation of Equation (2.70) was tested via numerical experiments in two-layer systems.

The convection in a porous medium confined in a horizontal cylinder with disk-shaped ends at different temperatures (Figure 2.11a) has features similar to the configuration of Figure 2.6. A parametric solution for the horizontal cylinder problem is reported in Bejan and Tien (1978). The corresponding phenomenon in a porous medium in the shape of a horizontal cylinder with annular cross-section (Figure 2.11b) is documented in Bejan and Tien (1979).

An important geometric configuration in thermal insulation engineering is the horizontal cylindrical annular space filled with fibrous or granular insulation (Figure 2.11c). In this configuration the heat transfer is oriented radially between the concentric cylindrical surfaces of radii r_i and r_o. Experimental

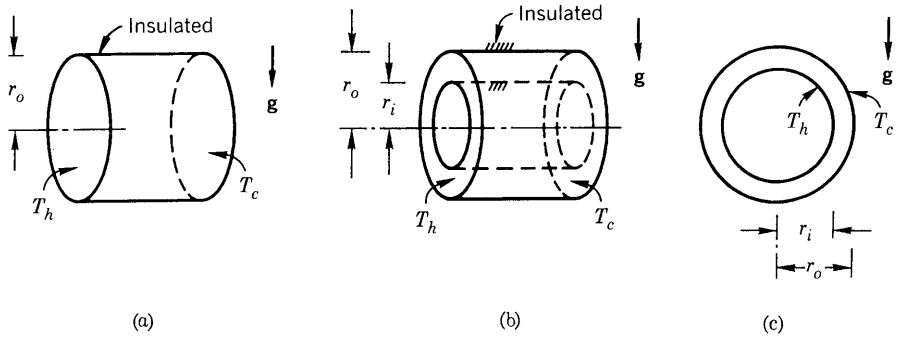

Fig. 2.11. Enclosures filled with porous media: (a) horizontal cylindrical enclosure; (b) horizontal cylindrical annulus with axial heat flow; (c) horizontal cylindrical annular enclosure, or spherical annulus, with radial heat flow.

measurements and numerical solutions for the overall heat transfer in the horizontal cylindrical annulus were reported in Caltagirone (1976) and Burns and Tien (1979). These results were correlated based on scale analysis in the range $1.19 \leq r_o/r_i \leq 4$ (Bejan, 1987),

$$\mathrm{Nu} = \frac{q'_{\text{actual}}}{q'_{\text{conduction}}} \approx 0.44\mathrm{Ra}_{r_i}^{1/2} \frac{\ln(r_o/r_i)}{1 + 0.916(r_i/r_o)^{1/2}}, \tag{2.71}$$

where $\mathrm{Ra}_{r_i} = Kg\beta r_i(T_h - T_c)/(\alpha\nu)$ and $q'_{\text{conduction}} = 2\pi k(T_h - T_c)/\ln(r_o/r_i)$. This correlation is valid in the convection-dominated limit, $\mathrm{Nu} \gg 1$.

Porous media confined to the space formed between two concentric spheres are also an important component in thermal insulation engineering. Figure 2.11c can be interpreted as a vertical cross-section through the concentric-sphere arrangement. Numerical heat transfer solutions for discrete values of Rayleigh number and radius ratio are reported graphically in Burns and Tien (1979). Using the method of scale analysis, the data that correspond to the convection-dominated regime ($\mathrm{Nu} \gtrsim 1.5$) have been correlated within 2% by the scaling-correct expression (Bejan, 1987)

$$\mathrm{Nu} = \frac{q_{\text{actual}}}{q_{\text{conduction}}} = 0.756\mathrm{Ra}_{r_i}^{1/2} \frac{1 - r_i/r_o}{1 + 1.422(r_i/r_o)^{3/2}}, \tag{2.72}$$

where $\mathrm{Ra}_{r_i} = Kg\beta r_i(T_h - T_c)/(\alpha\nu)$ and $q_{\text{conduction}} = 4\pi k(T_h - T_c)/(r_i^{-1} - r_o^{-1})$.

Natural convection through an annular porous insulation oriented vertically was investigated numerically (Havstad and Burns, 1982) and experimentally (Prasad *et al.*, 1985). These and other results are reviewed in Nield and Bejan (1999).

Natural convection in enclosures with heating from the side continues to attract interest. Heat and mass transfer (double diffusive convection) was studied by Mohamad and Bennacer (2002), Bera and Khalili (2002), Asbik *et al.* (2002), Benhadji and Vasseur (2001), Kalla *et al.* (2001), Bansod *et al.* (2000, 2002), and Rathish Kumar *et al.* (2002). An enclosure with a vertical fluid layer sandwiched between two porous layers was studied numerically by Bennacer *et al.* (2003). Enclosed porous media with heat generation were analyzed in Dhanasekaran *et al.* (2002) and Kim *et al.* (2001). The effect of variable porosity was documented in Marcondes *et al.* (2001). Natural convection in a partly porous cavity was described by Mercier *et al.* (2002). The effect of anisotropy was studied experimentally by Kimura *et al.* (2002).

2.10 Enclosures Heated from Below

The most basic configuration of a confined porous layer heated in the vertical direction is shown in Figure 2.12a. The most important difference between

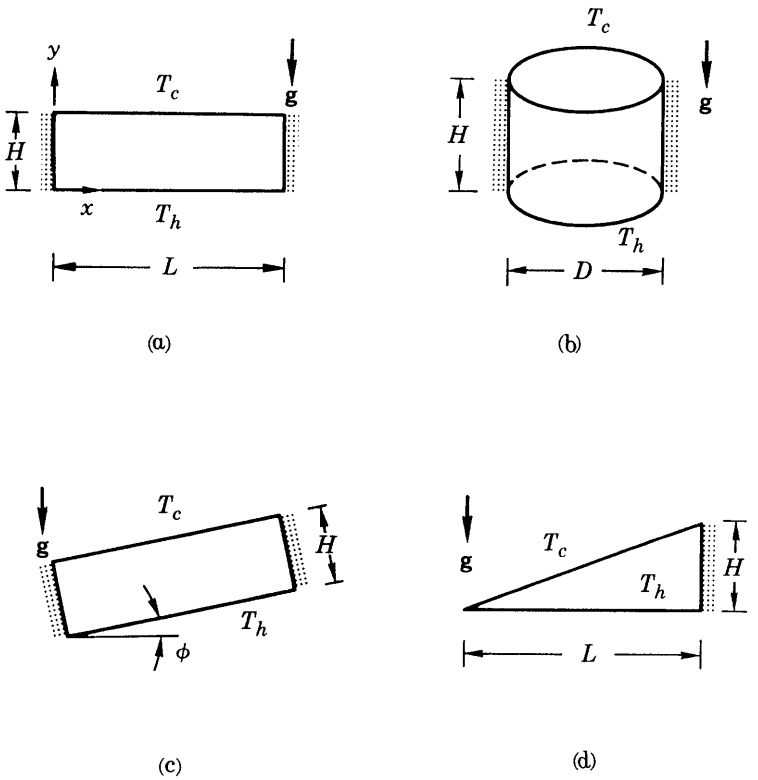

Fig. 2.12. Enclosed porous layers heated from below: (a) rectangular enclosure; (b) vertical cylindrical enclosure; (c) inclined rectangular enclosure; (d) wedge-shaped enclosure.

heat transfer in this configuration and heat transfer in confined layers heated from the side is that in Figure 2.12a convection occurs only when the imposed temperature difference or heating rate exceeds a certain finite value. Recall that in configurations such as Figure 2.6 convection is present even in the limit of vanishingly small temperature differences.

Assume that the fluid saturating the porous medium of Figure 2.12a expands upon heating ($\beta > 0$). By analogy with the phenomenon of Bénard convection in a pure fluid, in the convection regime the flow consists of finite-size cells that become more slender and multiply discretely as the destabilizing temperature difference $T_h - T_c$ increases. If $T_h - T_c$ does not exceed the critical value necessary for the onset of convection, the heat transfer mechanism through the layer of thickness H is that of pure thermal conduction. If the porous layer is heated from above (i.e., if T_h and T_c change places in Figure 2.12a), then the fluid remains stably stratified and the heat transfer is again due to pure thermal conduction: $q' = kL(T_h - T_c)/H$.

The onset of convection in an infinitely long porous layer heated from below was examined on the basis of linearized hydrodynamic stability analysis (Horton and Rogers, 1945; Lapwood, 1948; Nield and Bejan, 1999; Tyvand, 2002; Mamou, 2002). This subject continues to attract attention at the most fundamental level [e.g., Bilgen and Mbaye (2001) Rees (2002), and Banu and Rees (2002)]. For fluid layers confined between impermeable and isothermal horizontal walls, it was found that convection is possible if the Rayleigh number based on height exceeds the critical value

$$\mathrm{Ra}_H = \frac{Kg\beta H(T_h - T_c)}{\alpha\nu} = 4\pi^2 = 39.48. \tag{2.73}$$

A much simpler analysis based on constructal theory (Nelson and Bejan, 1998) predicted the critical Rayleigh number $12\pi = 37.70$, which approaches the hydrodynamic stability result within 5%. This analysis is summarized in Section 2.11. For a history of the early theoretical and experimental work on the onset of Bénard convection in porous media, and for a rigorous generalization of the stability analysis to convection driven by combined buoyancy effects, the reader is directed to Nield (1968), where it is shown that the critical Rayleigh number for the onset of convection in infinitely shallow layers depends to a certain extent on the heat and fluid flow conditions imposed along the two horizontal boundaries.

Of practical interest in heat transfer engineering is the heat transfer rate at Rayleigh numbers that are higher than critical. There has been a considerable amount of analytical, numerical, and experimental work devoted to this issue. Reviews of these advances may be found in Nield and Bejan (1999) and Cheng (1978). Constructal theory anticipates the entire curve relating heat transfer to Rayleigh number (Nelson and Bejan, 1998).

The scale analysis of the convection regime with Darcy flow (Bejan, 1984) indicates that the Nusselt number should increase linearly with the Rayleigh number, whence the relationship

$$\mathrm{Nu} \approx \frac{1}{40}\mathrm{Ra}_H \quad \text{for } \mathrm{Ra}_H > 40. \tag{2.74}$$

This linear relationship is confirmed by numerical heat transfer calculations at large Rayleigh numbers in Darcy flow (Kimura *et al.*, 1986). The experimental data compiled in Cheng (1978) show that the scaling law (2.74) serves as an upper bound for some of the high-Ra_H experimental data available in the literature.

Most of the data show that in the convection regime Nu increases as Ra_H^n, where n becomes progressively smaller than 1 as Ra_H increases. This behavior is anticipated by the constructal theory solution (Nelson and Bejan, 1998); see Section 2.11. The exponent $n \sim 1/2$ revealed by data at high Rayleigh numbers was anticipated based on a scale analysis of convection rolls in the

Forchheimer regime (Bejan, 1995a):

$$\frac{\mathrm{Nu}}{\mathrm{Pr}_p} \sim \left(\frac{\mathrm{Ra}_H}{\mathrm{Pr}_p}\right)^{1/2} \quad (\mathrm{Ra}_H > \mathrm{Pr}_p), \tag{2.75}$$

where Pr_p is the "porous medium Prandtl number" for the Forchheimer regime (Bejan, 1995a),

$$\mathrm{Pr}_p = \frac{H\nu}{bK\alpha} \tag{2.76}$$

and $b[m^{-1}]$ is defined in Equation (1.12). In this formulation Nu is a function of two groups, Ra_H and Pr_p, in which Pr_p accounts for the transition from Darcy to Forchheimer flow (Figure 2.13). In this formulation the Darcy flow result (2.74) becomes

$$\frac{\mathrm{Nu}}{\mathrm{Pr}_p} \sim \frac{1}{40}\frac{\mathrm{Ra}_H}{\mathrm{Pr}_p} \quad (40 < \mathrm{Ra}_H < \mathrm{Pr}_p). \tag{2.77}$$

The experimental data for convection in the entire regime spanned by the asymptotes given by Equations (2.75) and (2.77) are correlated by

$$\mathrm{Nu} = \left\{\left(\frac{\mathrm{Ra}_H}{40}\right)^n + [c(\mathrm{Ra}_H\mathrm{Pr}_p)^{1/2}]^n\right\}^{1/n}, \tag{2.78}$$

where $n = -1.65$ and $c = 1896$ are determined empirically based on measurements reported by many independent sources. The correlations of Equations (2.74) through (2.78) refer to layers with length/height ratios considerably greater than one. They apply when the length (lateral dimension L, perpendicular to gravity) of the confined system is greater than the horizontal length scale of a single convective cell, that is, greater than $H\mathrm{Ra}_H^{-1/2}$, according to the scale analysis of Bejan (1984).

These principles become partial effects in real-life systems that demand considerably more complex models. One important class for thermal and structural engineering are the cavernous walls and multiscale regenerators built with terra-cotta bricks. The terra-cotta material is porous, and moisture and heat diffuse together across it (Vasile *et al.*, 1998). The caverns can be designed to have many shapes, and they play host to a combination of natural convection and radiation (Lorente *et al.*, 1994, 1996). Furthermore, the thermal performance of the cavernous structure is in competition with the mechanical stiffness: from this competition emerges the optimal size and number of caverns (Lorente and Bejan, 2002). This subject is treated in some detail in Section 8.1.

Natural-convection studies have also been reported for porous layers confined in rectangular parallelepipeds heated from below, horizontal circular cylinders, and horizontal annular cylinders. The general conclusion is that the lateral walls have a convection-suppression effect. For example, in a circular

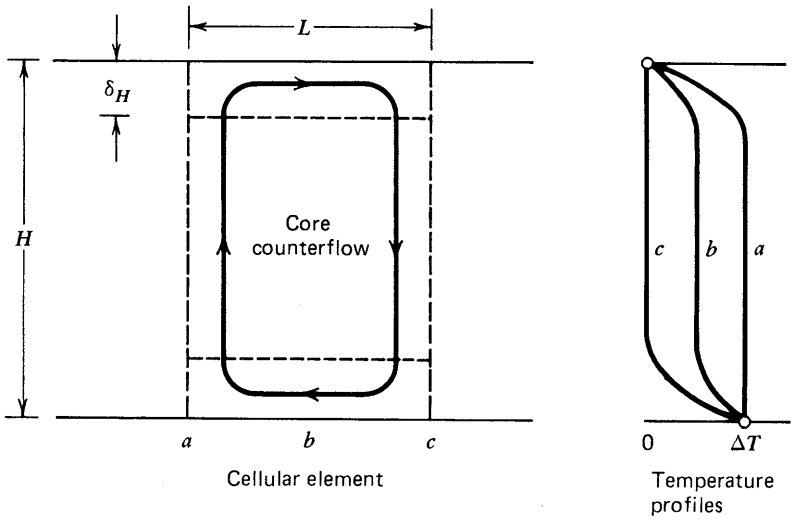

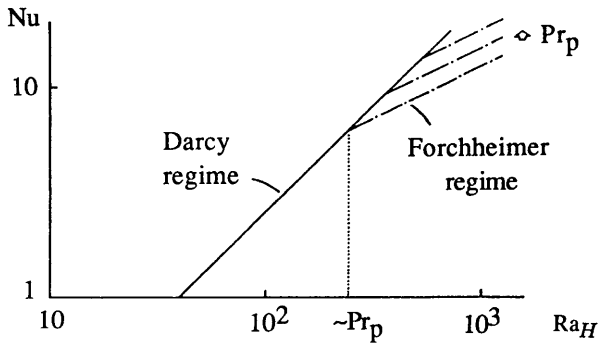

Fig. 2.13. Convective heat transfer in a porous layer heated from below, in the Darcy and Forchheimer regimes (Bejan, 1995a; from Bejan, *Convection Heat Transfer*, 2nd ed., Copyright © 1995 Wiley. This material is used by permission of John Wiley & Sons, Inc.).

cylinder of diameter D and height H (Figure 2.12b), in the limit $D \ll H$ the critical condition for the onset of convection is (Bau and Torrance, 1982)

$$\mathrm{Ra}_H = 13.56 \left(\frac{H}{D}\right)^2. \tag{2.79}$$

In porous layers inclined from the horizontal position at an angle ϕ (Figure 2.12c), convection sets in at Rayleigh numbers that satisfy the

criterion (Combarnous and Bories, 1975)

$$\mathrm{Ra}_H > \frac{39.48}{\cos\phi}, \tag{2.80}$$

where it is assumed that the boundaries are isothermal and impermeable. The average heat transfer rate at high Rayleigh numbers can be estimated by

$$\mathrm{Nu} = 1 + \sum_{s=1}^{\infty} k_s \left(1 - \frac{4\pi^2 s^2}{\mathrm{Ra}_H \cos\phi}\right), \tag{2.81}$$

where $k_s = 0$ if $\mathrm{Ra}_H \cos\phi < 4\pi^2 s^2$, and $k_s = 2$ if $\mathrm{Ra}_H \cos\phi \geq 4\pi^2 s^2$.

In a porous medium confined in a wedge-shaped (or attic-shaped) space cooled from above (Figure 2.12d), convection consisting of a single counterclockwise cell exists even in the limit $\mathrm{Ra}_H \to 0$, because in this direction the imposed heating is not purely vertical. The same observation holds for Figure 2.12c. Numerical solutions of transient high Rayleigh number convection in wedge-shaped layers show the presence of a Bénard-type instability at high enough Rayleigh numbers (Poulikakos and Bejan, 1983b). When $H/L = 0.2$, the instability occurs above $\mathrm{Ra}_H \cong 620$. It was found that this critical Rayleigh number increases as H/L increases.

Nuclear-safety issues have motivated the study of natural convection in horizontal saturated porous layers (Figure 2.12a) heated volumetrically at a rate q'''. Boundary conditions and observations regarding the onset of convection and overall Nusselt numbers are presented in Nield and Bejan (1999). It is found that convection sets in at internal Rayleigh numbers Ra_I in the range 33 to 46 (Kulacki and Freeman, 1979), where

$$\mathrm{Ra}_I = \frac{g\beta H^3 K q'''}{2k\alpha\nu_f} \tag{2.82}$$

and the subscript f indicates properties of the fluid alone. Top and bottom surface temperature experimental measurements in the convection-dominated regime ($10^3 < \mathrm{Ra}_I < 10^4$) are adequately represented by (Buretta and Berman, 1976)

$$\frac{q''' H^2}{2k(T_h - T_c)} \approx 0.116 \mathrm{Ra}_I^{0.573}, \tag{2.83}$$

where T_h and T_c are the resulting bottom and top temperatures when q''' is distributed throughout the layer of Figure 2.12a.

2.11 The Method of Intersecting the Asymptotes

In this section we take a closer look at the phenomenon of convection in a porous layer heated from below. Our objective is to show that most of the

features of the flow can be determined based on a simple method: the intersection of asymptotes (Nelson and Bejan, 1998). This method was originally used for the optimization of spacings for compact cooling channels for electronics (Bejan, 1984), as we show in Sections 5.2 and 5.3. See also Lewins (2003).

Assume that the system of Figure 2.14 is a porous layer saturated with fluid and that, if present, the flow is two-dimensional and in the Darcy regime. The height H is fixed, and the horizontal dimensions of the layer are infinite in both directions. The fluid has nearly constant properties such that its density–temperature relation is described well by the Boussinesq linearization. The volume-averaged equations that govern the conservation of mass, momentum, and energy are

$$\frac{\partial u}{\partial x}+\frac{\partial v}{\partial y}=0, \tag{2.84}$$

$$\frac{\partial u}{\partial y}-\frac{\partial v}{\partial x}=-\frac{Kg\beta}{\nu}\frac{\partial T}{\partial x}, \tag{2.85}$$

$$u\frac{\partial T}{\partial x}+v\frac{\partial T}{\partial y}=\alpha\left(\frac{\partial^2 T}{\partial x^2}+\frac{\partial^2 T}{\partial y^2}\right). \tag{2.86}$$

The horizontal length scale of the flow pattern ($2L_r$), or the geometric aspect ratio of one roll, is unknown. The method consists of analyzing two extreme flow configurations—many counterflows versus few plumes—and intersecting these asymptotes for the purpose of maximizing the global thermal conductance of the flow system [cf. constructal theory, Bejan (2000)].

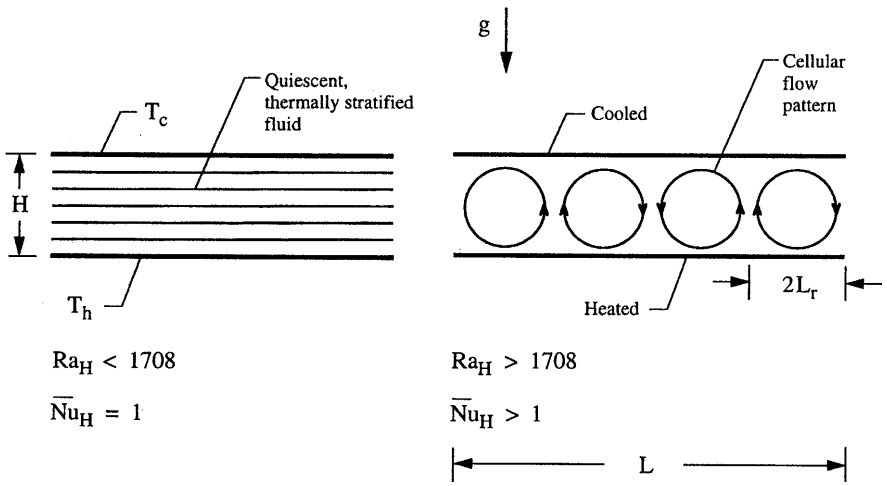

Fig. 2.14. Horizontal porous layer saturated with fluid and heated from below (Nelson and Bejan, 1998).

2.11.1 The Many Counterflows Regime

In the limit $L_r \to 0$ each roll is a very slender vertical counterflow, as shown in Figure 2.15. Because of symmetry, the outer planes of this structure ($x = \pm L_r$) are adiabatic: they represent the center planes of the streams that travel over the distance H. The scale analysis of the $H \times (2L_r)$ region indicates that in the $L_r/H \to 0$ limit the horizontal velocity component u vanishes. This scale analysis is not shown because it is well known as the defining statement of fully developed flow [e.g., Bejan (1995a, p. 97)]. Equations (2.85) and (2.86) reduce to

$$\frac{\partial v}{\partial x} = \frac{Kg\beta}{\nu}\frac{\partial T}{\partial x}, \tag{2.87}$$

$$v\frac{\partial T}{\partial y} = \alpha\frac{\partial^2 T}{\partial x^2}, \tag{2.88}$$

which can be solved exactly for v and T. The boundary conditions are $\partial T/\partial x = 0$ at $x = \pm L_r$, and the requirement that the extreme (corner) temperatures of the counterflow region are dictated by the top and bottom walls, $T(-L_r, H) = T_c$ and $T(L_r, 0) = T_h$. The solution is given by

$$v(x) = \frac{\alpha}{2H}\left[\mathrm{Ra}_H - \left(\frac{\pi H}{2L_r}\right)^2\right]\sin\left(\frac{\pi x}{2L_r}\right), \tag{2.89}$$

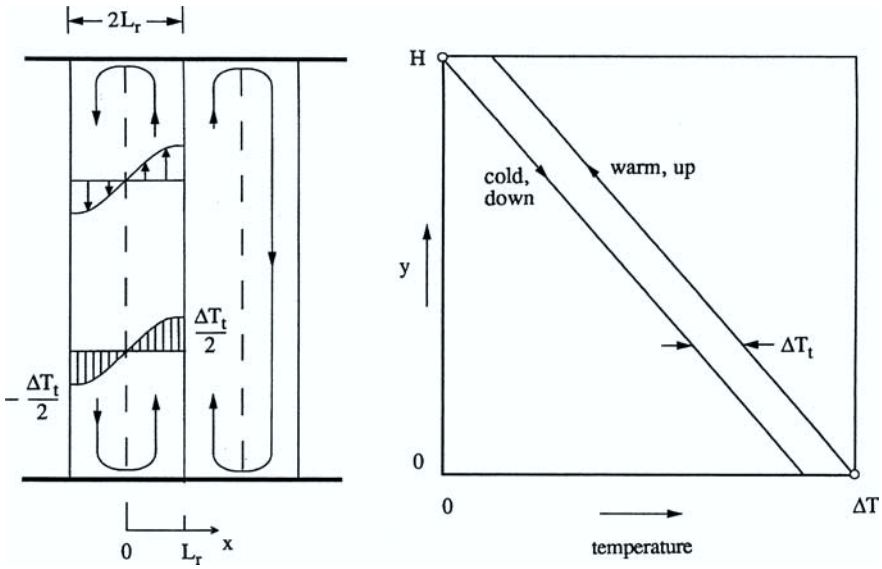

Fig. 2.15. The extreme in which the flow consists of many vertical and slender counterflows (Nelson and Bejan, 1998).

$$T(x,y) = \frac{\nu}{Kg\beta}v(x) + \frac{\nu}{Kg\beta}\left(2\frac{y}{H} - 1\right)\frac{\alpha}{2H}\left[\mathrm{Ra}_H - \left(\frac{\pi H}{2L_r}\right)^2\right] + (T_h - T_c)\left(1 - \frac{y}{H}\right), \tag{2.90}$$

where the porous-medium Rayleigh number $\mathrm{Ra}_H = Kg\beta H(T_h - T_c)/(\alpha\nu)$ is a specified constant. The right side of Figure 2.15 shows the temperature distribution along the vertical boundaries of the flow region ($x = \pm L_r$): the vertical temperature gradient $\partial T/\partial y$ is independent of altitude. The transversal (horizontal) temperature difference (ΔT_t) is also a constant,

$$\Delta T_t = T(x = L_r) - T(x = -L_r) = \frac{\nu}{Kg\beta}\frac{\alpha}{H}\left[\mathrm{Ra}_H - \left(\frac{\pi H}{2L_r}\right)^2\right]. \tag{2.91}$$

The counterflow convects heat upward at the rate q', which can be calculated using Equations (2.89) and (2.90):

$$q' = \int_{-L}^{L} (\rho c_P)_f v T \, dx. \tag{2.92}$$

The average heat flux convected in the vertical direction, $q'' = q'/(2L_r)$, can be expressed as an overall thermal conductance

$$\frac{q''}{\Delta T} = \frac{k}{8H\mathrm{Ra}_H}\left[\mathrm{Ra}_H - \left(\frac{\pi H}{2L_r}\right)^2\right]^2. \tag{2.93}$$

This result is valid provided the vertical temperature gradient does not exceed the externally imposed gradient, $(-\partial T/\partial y) < \Delta T/H$. This condition translates into

$$\frac{L_r}{H} > \frac{\pi}{2}\mathrm{Ra}_H^{-1/2}, \tag{2.94}$$

which in combination with the assumed limit $L_r/H \to 0$ means that the domain of validity of Equation (2.93) widens when Ra_H increases. In this domain the thermal conductance $q''/\Delta T$ decreases monotonically as L_r decreases [cf. Figure 2.16].

2.11.2 The Few Plumes Regime

As L_r increases, the number of rolls decreases and the vertical counterflow is replaced by a horizontal counterflow in which the thermal resistance between T_h and T_c is dominated by two horizontal boundary layers, as in Figure 2.17. Let δ be the scale of the thickness of the horizontal boundary layer. The thermal conductance $q''/\Delta T$ can be deduced from the heat transfer solution for

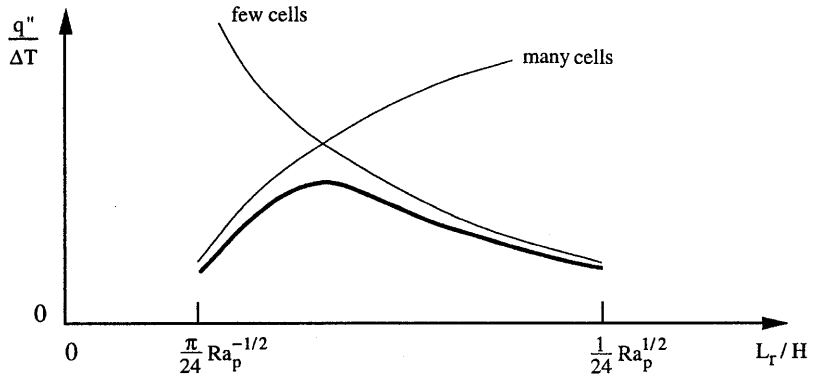

Fig. 2.16. The geometric maximization of the thermal conductance of a fluid-saturated porous layer heated from below (Nelson and Bejan, 1998).

natural convection boundary layer flow over a hot isothermal horizontal surface facing upward, or a cold surface facing downward. The similarity solution for the horizontal surface with power-law temperature variation (Cheng and Chang, 1976) can be used to develop an analytical result, as we show at the end of this section. Plume flows have also been described by Shu and Pop (1997).

A simpler analytical solution can be developed in a few steps using the integral method. Consider the slender flow region $\delta \times (2L_r)$, where $\delta \ll 2L_r$, and integrate Equations (2.84) to (2.86) from $y = 0$ to $y \to \infty$, that is, into the region just above the boundary layer. The surface temperature is T_h, and the temperature outside the boundary layer is T_∞ (constant). The origin $x = 0$ is set at the tip of the wall section of length $2L_r$. The integrals of Equations (2.84) and (2.86) yield

$$\frac{d}{dx}\int_0^\infty u(T - T_\infty)dy = -\alpha\left(\frac{\partial T}{\partial y}\right)_{y=0}. \tag{2.95}$$

The integral of Equation (2.85), in which we neglect $\partial v/\partial x$ in accordance with boundary layer theory, leads to

$$u_0(x) = \frac{Kg\beta}{\nu}\frac{d}{dx}\int_0^\infty T\,dy, \tag{2.96}$$

where u_0 is the velocity along the surface, $u_0 = u(x, 0)$. Reasonable shapes for the u and T profiles are the exponentials

$$\frac{u(x,y)}{u_0(x)} = \exp\left[-\frac{y}{\delta(x)}\right] = \frac{T(x,y) - T_\infty}{T_h - T_\infty} \tag{2.97}$$

which transform Equations (2.95) and (2.96) into

$$\frac{d}{dx}(u_0\delta) = \frac{2\alpha}{\delta}, \tag{2.98}$$

$$u_0 = \frac{Kg\beta}{\nu}(T_h - T_\infty)\frac{d\delta}{dx}. \tag{2.99}$$

These equations can be solved for $u_0(x)$ and $\delta(x)$,

$$\delta(x) = \left[\frac{9\alpha\nu}{Kg\beta(T_h - T_\infty)}\right]^{1/3} x^{2/3}. \tag{2.100}$$

The solution for $u_0(x)$ is of the type $u_0 \sim x^{-1/3}$, which means that the horizontal velocities are large at the start of the boundary layer, and decrease as x increases. This is consistent with the geometry of the $H \times 2L_r$ roll sketched in Figure 2.17, where the flow generated by one horizontal boundary layer turns the corner and flows vertically as a relatively narrow plume (narrow relative to $2L_r$), to start with high velocity (u_0) a new boundary layer along the opposite horizontal wall.

The thermal resistance of the geometry of Figure 2.17 is determined by estimating the local heat flux $k(T_h - T_\infty)/\delta(x)$ and averaging it over the total length $2L_r$:

$$q'' = \left(\frac{3}{4}\right)^{1/3} \frac{k\Delta T}{H} \left(\frac{T_h - T_\infty}{\Delta T}\right)^{4/3} \mathrm{Ra}_H^{1/3} \left(\frac{H}{L_r}\right)^{2/3}. \tag{2.101}$$

The symmetry of the sandwich of boundary layers requires $T_h - T_\infty = (1/2)\Delta T$, such that

$$\frac{q''}{\Delta T} = \frac{3^{1/3}k}{4H}\mathrm{Ra}_H^{1/3} \left(\frac{H}{L_r}\right)^{2/3}. \tag{2.102}$$

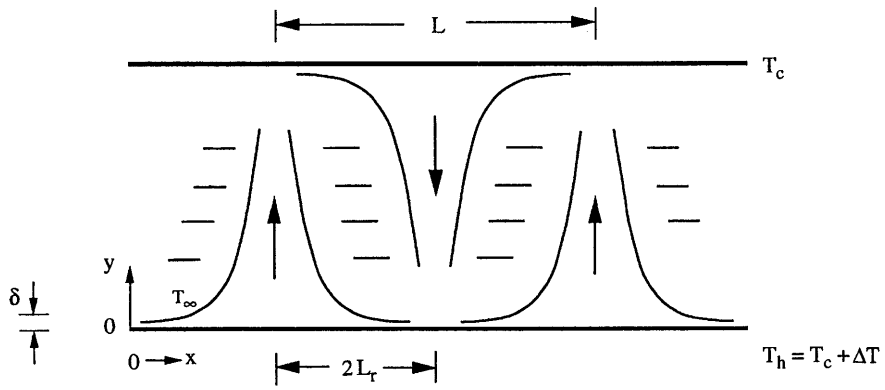

Fig. 2.17. The extreme in which the flow consists of a few isolated plumes (Nelson and Bejan, 1998).

The goodness of this result can be tested against the similarity solution for a hot horizontal surface that faces upward in a porous medium and has an excess temperature that increases as x^λ. The only difference is that the role that was played by $(T_h - T_\infty)$ in the preceding analysis is now played by the excess temperature averaged over the surface length $2L_r$. If we use $\lambda = 1/2$, which corresponds to uniform heat flux, then it can be shown that the solution of Cheng and Chang (1976) leads to the same formula as Equation (2.102), except that the factor $3^{1/3} = 1.442$ is replaced by $0.816(3/2)^{4/3} = 1.401$. Equation (2.102) is valid when the specified Ra_H is such that the horizontal boundary layers do not touch. We write this geometric condition as $\delta(x = 2L_r) < H/2$ and, using Equation (2.100), we obtain

$$\frac{L_r}{H} < \frac{1}{24}\mathrm{Ra}_H^{1/2}. \tag{2.103}$$

Since in this analysis L_r/H was assumed to be very large, we conclude that the L_r/H domain in which Equation (2.102) is valid becomes wider as the specified Ra_H increases. The important feature of the "few rolls" limit is that the thermal conductance decreases as the horizontal dimension L_r increases. This second asymptotic trend has been added to Figure 2.16.

2.11.3 The Intersection of Asymptotes

Figure 2.16 presents a bird's-eye view of the effect of flow shape on thermal conductance. Even though we did not draw $q''/\Delta T$ completely as a function of L_r, the two asymptotes tell us that the thermal conductance is maximum at an optimal L_r value that is close to their intersection. There is a family of such curves, one curve for each Ra_H. The $q''/\Delta T$ peak of the curve rises, and the L_r domain of validity around the peak becomes wider as Ra_H increases. Looking in the direction of small Ra_H values we see that the domain vanishes (and the cellular flow disappears) when the following requirement is violated,

$$\frac{1}{24}H\mathrm{Ra}_H^{1/2} - \frac{\pi}{2}H\mathrm{Ra}_H^{-1/2} \geq 0. \tag{2.104}$$

This inequality means that the flow exists when $\mathrm{Ra}_H \geq 12\pi = 37.70$. This conclusion is extraordinary: it agrees with the stability criterion for the onset of two-dimensional convection, Equation (2.73), namely, $\mathrm{Ra}_H > 4\pi^2 = 39.5$, which was derived based on a lengthier analysis and the assumption that a flow structure exists, the initial disturbances (Horton and Rogers, 1945; Lapwood, 1948).

We obtain the optimal shape of the flow $2L_{r,\mathrm{opt}}/H$, by intersecting the asymptotes (2.93) and (2.102):

$$\pi^2\left(\frac{H}{2L_{r,\mathrm{opt}}}\mathrm{Ra}_H^{-1/2}\right)^2 + 2^{5/6}3^{1/6}\left(\frac{H}{2L_{r,\mathrm{opt}}}\mathrm{Ra}_H^{-1}\right)^{1/3} = 1. \tag{2.105}$$

Over most of the Ra_H domain where Equation (2.104) is valid, Equation (2.105) is well approximated by its high Ra_H asymptote:

$$\frac{2L_{r,\mathrm{opt}}}{H} \cong \pi \mathrm{Ra}_H^{-1/2}. \tag{2.106}$$

The maximum thermal conductance is obtained by substituting the $L_{r,\mathrm{opt}}$ value in either Equation (2.102) or Equation (2.93). This estimate is an upper bound, because the intersection is above the peak of the curve. In the high-Ra_H limit (2.106) this upper bound assumes the analytical form

$$\left(\frac{q''}{\Delta T}\right)_{\max} \frac{H}{k} \lesssim \frac{3^{1/3}}{2^{4/3}\pi^{2/3}} \mathrm{Ra}_H^{2/3}. \tag{2.107}$$

Towards lower Ra_H values the slope of the $(q''/\Delta T)_{\max}$ curve increases such that the exponent of Ra_H approaches 1. This behavior is in excellent agreement with the large volume of experimental data collected for Bénard convection in saturated porous media (Cheng, 1978). The less-than-1 exponent of Ra_H in the empirical $\mathrm{Nu}(\mathrm{Ra}_H)$ curve, and the fact that this exponent decreases as Ra_H increases, has attracted considerable attention from theoreticians during the last two decades (Nield and Bejan, 1999).

In this section and Sections 2.2 and 2.5, we outlined the basic rule for two methods of solution for problems of convection in porous media: scale analysis and the intersection of asymptotes. These are two of the simplest methods that are available. They yield concrete results for engineering problems such as heat transfer rates, flow rates, velocities, temperature differences, and time intervals. They distinguish themselves from other methods because they offer a high return on investment: because they are so simple, they deserve to be tried first, as preliminaries, even in problems where more exact results are needed. Simple methods identify the proper dimensionless formulation for presenting more exact (and more expensive) results developed based on more complicated methods (analytical, numerical, and/or experimental).

Other simple methods are available, for example, the integral method (Karman–Pohlhausen), Equations (2.95) to (2.100), and similarity formulations [e.g., Bejan (1995a)]. A word of caution goes with the use of all "simple" methods. More complicated problems with nonsimilar and singular solutions may require more advanced treatments from the start.

The intersection of asymptotes method relied on an additional principle that applies throughout the physics of flow systems: the constructal law, the generation of flow geometry for the maximization of access for currents in systems far from equilibrium. In Figure 2.16, we invoked this principle when we minimized the global thermal resistance encountered by the flow of heat across the horizontal porous layer. The intersection of the two asymptotes is an approximation of the flow geometry that minimizes the global thermal resistance. The same "constructal principle" has been used to predict flow

geometry and transitions between flow regimes in a great variety of configurations (Bejan, 2000).

The most important conclusion is that by learning simple methods, and using them correctly, the young researcher learns two important lessons. One is "try the simplest first." Simple methods are valuable throughout thermal and fluid sciences, not only in porous media. The other lesson is the open competition among methodologies in the search for engineering answers to fundamental questions. A researcher with a personal mathematics background and, most important, with a personal supply of curiosity and time can and should judiciously evaluate the worthiness of any of these methodologies relative to his or her ability and taste (Bejan, 1995a, p. 55).

http://www.springer.com/978-0-387-20225-9

Porous and Complex Flow Structures in Modern Technologies

Bejan, A.; Dincer, I.; Lorente, S.; Miguel, A.; Reis, H.

2004, XII, 396 p. 49 illus., Hardcover
ISBN: 978-0-387-20225-9